A Geometric Multiscale modelling approach to the analysis of MSR plant dynamics

Matteo Zanetti [a], Antonio Cammi [a], Carlo Fiorina [b], Lelio Luzzi [a, *]

[a] Politecnico di Milano, Department of Energy, CeSNEF (Enrico Fermi Center for Nuclear Studies), via La Masa 34, 20156 Milano, Italy
[b] Paul Scherrer Institute, Laboratory for Reactor Physics and Systems Behavior, FAST Group 5232, Villigen PSI, Switzerland

Received 4 August 2014
Received in revised form
4 February 2015
Accepted 27 February 2015
Available online

1. Introduction

The Molten Salt Reactor (MSR) is one of the six innovative reactors considered in the framework of the Generation IV International Forum (GIF, 2002, 2014; Serp et al., 2014) as a possible answer to the compelling need of a safer and sustainable nuclear energy production. The MSR is particularly promising for actinide burning and waste management (Fiorina et al., 2013), two of the main concerns of the modern nuclear industry. The main feature of MSRs is the presence of a molten fuel, which circulates through the core and out of it, in one or more heat exchangers. The liquid nature of the fuel also allows important improvement from the safety point of view (e.g., see Luzzi et al., 2012a; Krepel et al., 2014a). For instance, continuous adjustment of the fuel composition is possible, avoiding the need of reactivity reserve and thus reducing the risks associated to an accidental reactivity insertion. Thanks to the high boiling temperature of the molten salt, high temperatures can be reached with low core internal pressures, reducing the problems of mechanical stresses on the structural elements.

Following the inherent flexibility of a liquid-fuelled reactor, different MSR configurations have been proposed in the past. Among them, it is possible to distinguish two main kinds of MSRs, i.e., with and without a moderator (typically graphite). On one hand, many efforts are presently being put in the development of a fast-spectrum MSR (Mathieu et al., 2009; Renault et al., 2009; Merle-Lucotte et al., 2011; Serp et al., 2014), where no graphite is present in the core, and where the neutron spectrum is softened only by the fuel salt itself. For example, the Molten Salt Fast Reactor, developed in the framework of the Euratom EVOL Project,[1] has the advantage of a good neutron economy for both fissile breeding and actinide burning, and is characterized by high safety margins in

* Corresponding author.
E-mail address: lelio.luzzi@polimi.it (L. Luzzi).

[1] http://www.evol-project.org/.

terms of temperature reactivity feedback (Mathieu et al., 2006; Merle-Lucotte et al., 2008). Moreover, the absence of graphite removes the problems connected to its damage and possible replacement as well as to its handling as a massive radioactive waste. On the other hand, two MSR prototypes have been built in the past at Oak Ridge National Laboratory (ORNL) – namely, the Aircraft Reactor Experiment (ARE) and the Molten Salt Reactor Experiment (MSRE) (Haubenreich and Engel, 1970; MacPherson, 1985) – and both made use of a moderator. In particular, the MSRE was built as a first step towards the realization of an electricity-producing MSR, and adopted a graphite core for neutron moderation. The construction and operation of the MSRE made possible the set-up of a sound technical basis for the design of commercial reactors. Relying upon this basis, many R&D programs have been carried out in the past. Among these, it must be cited the design of the Molten Salt Breeder Reactor (MSBR) (MacPherson, 1985) developed at the ORNL during the seventies. In the eighties, an R&D program was started in Japan for the realization of a graphite-moderated reactor called FUJI (Furukawa et al., 2008). Other activities are carried out for instance in Canada (LeBlanc, 2010), Czech Republic (Hron, 2005; Uhlíř, 2007), China (Serp et al., 2014), along with theoretical studies performed in Switzerland (Krepel et al., 2014a,b).

Hence, despite the shift of the GIF-IV interest towards the fast-spectrum configuration, graphite-moderated MSRs are still characterized by a widespread consideration. In addition, the presence of experimental and design data is fundamental for the assessment of models able to describe MSR behaviour. For these reasons, graphite-moderated MSRs have been considered also in this paper, which is aimed at the development of a suitable simulation tool for analyzing MSR dynamics. The need for new and reliable tools derives from the particular nature of the MSRs, in which a single fluid acts both as fuel and coolant. This double role gives rise to peculiar phenomena like: i) the drift and out-of-core decay of the Delayed Neutron Precursors (DNPs), that reduce the prompt criticality margin due to the loss of a fraction of the delayed neutrons produced into the core; ii) heat transfer involving a heat-generating fluid. These aspects lead to a complex and highly-coupled phys-ical environment that cannot be addressed using modelling approaches and codes developed for solid-fuelled nuclear reactors without major modifications of their structure.

Efforts in the development of suitable simulation tools were made by different authors and for a variety of molten salt systems (Mylonakis et al., 2014), but most of the studies carried out are featured by various simplifying hypotheses, such as assuming known velocities (Lapenta et al., 2001; Dulla et al., 2004; Dulla and Ravetto, 2007), one-dimensional flow and simplified heat transfer models (Lecarpentier and Carpentier, 2003; Yamamoto et al., 2005, 2006; Krepel et al., 2014a, 2005, 2007; Suzuki and Shimazu, 2006, 2008; Kópházi et al., 2009; Zhang et al., 2009a,c), simple cross-section feedback (Nicolino et al., 2008), only steady-state conditions (Wang et al., 2006; Zhang et al., 2009b). Recently, coupled approaches have been developed for the modelling of neutronics, heat transfer and fluid-dynamics, either by coupling a multiple-channel thermal-hydraulic analysis code with a Monte Carlo neutronic code (Guo et al., 2013) or by solving directly the governing equations in a multi-dimensional domain (Nagy et al., 2014; Zhang et al., 2014). Several activities on the last subject have also been carried out in the past at the Politecnico di Milano (Fiorina et al., 2010; Guerrieri et al., 2010, 2011; Cammi et al., 2011a,b, 2012; Luzzi et al., 2012b; Fiorina et al., 2014; Aufiero et al., 2014b). These activities have confirmed the need of dedicated simulation tools and have suggested the adoption of an innovative modelling approach based on the simultaneous solution, in the same computational environment, of the Partial Differential Equations (PDE) governing the physical phenomena involved in the MSR dynamics. This Multi-Physics Modelling (MPM) approach has been proved able to give unique information on the peculiar aspects of the MSR behaviour (Cammi et al., 2011b, 2012; Aufiero et al., 2014b), but requires a huge amount of computational po-wer when complex, 3-D geometries are considered.

In this paper, the Geometric Multiscale (GM) approach (Quarteroni and Veneziani, 2003) is adopted for MSR dynamics, showing how the different characteristics of this kind of reactor can be taken into account to build a "hybrid" multi-physics model. The GM approach consists in modelling different "components" of a system with respect to their dimensionality, meaning that, for example, straight tubes can be modelled with 1-D description while pool-like components can be addressed in full three dimensions. We can extend this intention to choose a different level of detail for modelling components that are considered less or more important for the overall model or that require some physical phenomena to be modelled with more accuracy. In our case, 3-D MP models (based on PDEs) will be connected to simpler 0-D ones based on Ordinary Differential Equations (ODEs), so that the boundary conditions for the MP part can be determined for each time-step taking into account the behaviour of the whole plant.

The MSRE layout was chosen as reference configuration because of the availability of both design and experimental data. In particular, the GM model developed for the MSRE considers the core as subdivided in three radial zones, each one described by means of a 3-D MP modelled channel, while the out-of-core components are described by means of lumped capacitance models (0-D). By adopting the described approach, we aim to conjugate the accuracy of the MPM approach with acceptable computation loads, by modelling with full accuracy the only parts for which it is necessary. The GM model has been developed for power-range conditions, in which the coupling between different physics has to be carefully modelled. Preliminary results of a simplified GM model have been presented in Zanetti et al. (2014).

The paper is organized as follows. In Section 2, the MSRE layout and data are introduced. In Section 3, the GM approach is presented. Section 4 deals with the description of the GM model adopted for the MSRE plant. In Section 5, some reactivity insertion transient simulations are reported, and the results are compared to experimental data for validation. Finally, the main conclusions are drawn in Section 6.

2. MSRE layout and data

The MSRE was an 8 MW_{th} prototype of graphite-moderated reactor built at ORNL to investigate the feasibility of the molten salt reactor technology for civil application. The core was composed by graphite blocks arranged in order to form channels with rectangular cross section, smoothed on the edges (Fig. 1). In these channels, laminar flow was established. The fluid was a fluoride salt containing the fissile material. Both ^{233}U and ^{235}U were used during the operational period of the MSRE. In this paper, the considered composition is 65% LiF, 29.1% BeF_2, 5.0% ZrF_4, and 0.9% UF_4, with ^{233}U as fissile material. The heat generated inside the core was transported through a heat exchanger to a secondary circuit still working with a mixture of fluoride salts and was then dissipated in the environment by means of a radiator.

A schematic representation of the plant layout is reported in Fig. 2.

3. Geometric Multiscale modelling approach

The MPM approach can be defined as the node-wise implicitly-coupled solution of a number of PDEs in a multi-dimensional

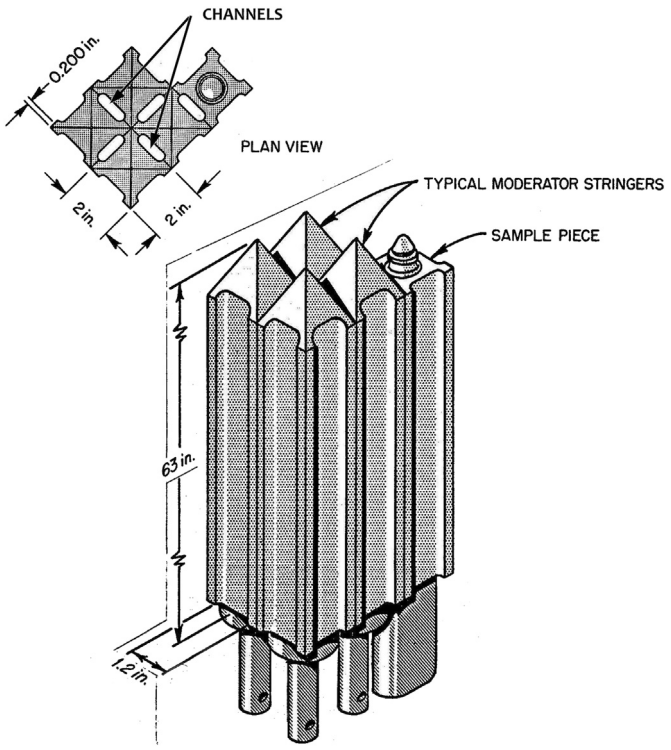

Fig. 1. Schematic representation of the MSRE graphite blocks and channel arrangement (Kedl, 1970).

domain. It is aimed at a precise and point-wise coupled description of the physical phenomena involved in a considered system, giving a unique insight into its dynamics. On the other hand, the MPM approach inevitably leads to notable computational requirements, which ask for simplified geometries. In this work, we show how the Geometric Multiscale approach can be used to obtain MP accuracy with an acceptable computational burden. The GM modelling approach consists in the representation of the components of a system on the basis of the relevance of the physical phenomena, namely: important components or those requiring tightly coupled solutions are investigated using 3-D MP models, while the other ones are represented using simplified (typically 0-D) models. The components featuring different dimensional representations are then connected by means of appropriate boundary conditions. From the perspective of the MP models, this means that the non-modelled part of the system is represented by realistic boundary conditions, which take into account the behaviour of the whole system. The GM approach allows building flexible and modular models, since the various modelling parts can be easily replaced with higher or lower detailed ones or new components can be easily added to expand the overall model.

The GM model of the MSRE presented in this work can be considered as a reduced version of a fully MP model of the reactor, whose implementation would consist in highly intensive computations, if even feasible. The core is modelled by 3-D channels, whose boundary conditions are handled by ODE-based 0-D models representative of the other system components, so that the reactor and its cooling loop can be described with different levels of detail. Such approach can be considered similar to the one developed in Quarteroni and Veneziani (2003) for the cardiovascular system: in short, very small arteries are modelled on one/zero dimension, whereas for the heart a 3-D model is used. Other similar approaches have been developed in the recent years through the coupling of system codes with CFD ones, as reported in Mengali et al. (2012).

In particular, our approach is implemented through the coupling between the MP code COMSOL Multiphysics® (Comsol, 2012b) and the control-oriented environment MATLAB® Simulink (Matlab, 2012). The main advantage of the choice of these two software

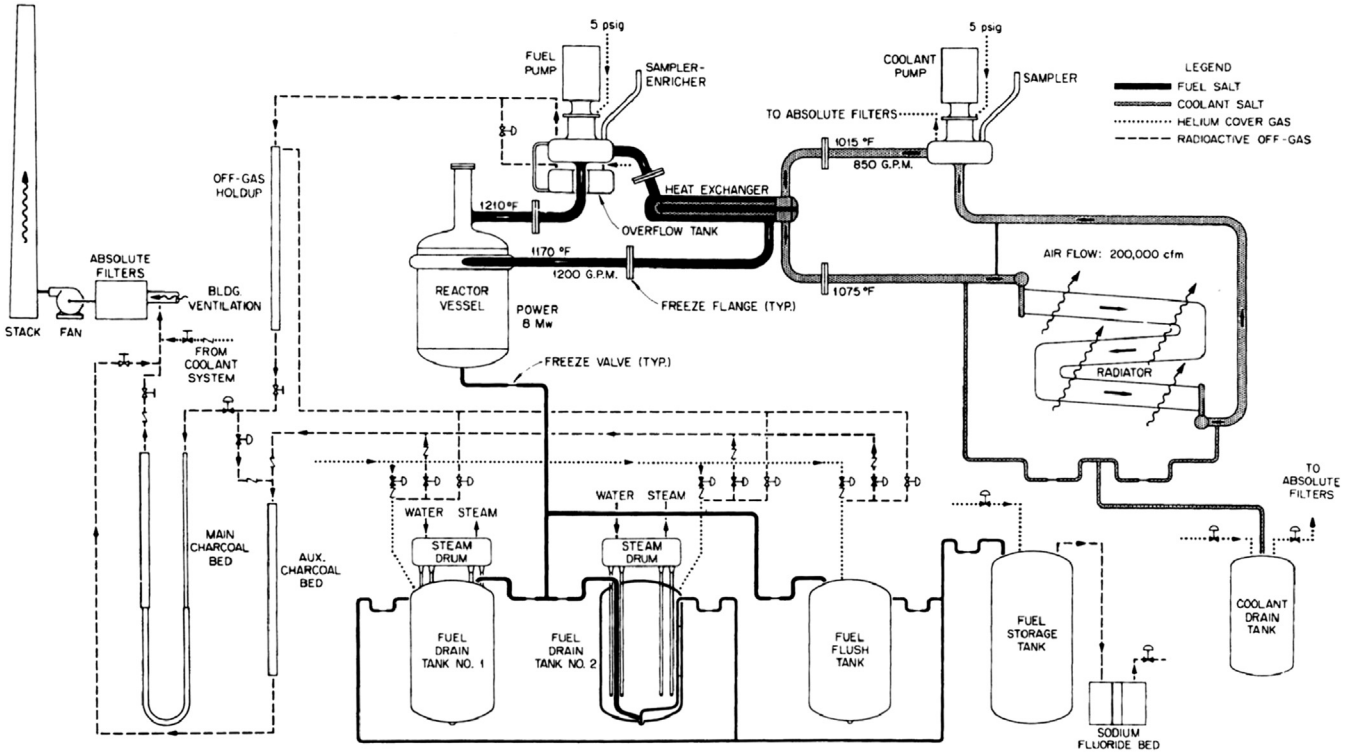

Fig. 2. Schematic representation of the MSRE plant layout (Guymon, 1973).

platforms is the native interface-ability of COMSOL with MATLAB (that does not require an interface program as with coupled codes), as well as the availability of a large library dedicated to detailed simulation and control in Simulink. Thus, if the GM model is properly settled, exploiting the modelling flexibility, it can be used for control-oriented applications. According to the authors' knowledge, only three examples of a similar software coupling exist in literature (Fütterer, 2008; Schijndel, 2009; Li and Yang, 2010).

4. MSRE plant Geometric Multiscale model

In this section, the MSRE plant model based on the Geometric Multiscale approach is presented. In the GM MSRE model, the selected MP components are the reactor channels, while the remaining part of the reactor plant is modelled by means of 0-D models of its constituents. A conceptual scheme of the overall GM model is presented in Fig. 3.

For the construction of the overall model, we started from a stand-alone MP description of a generic reactor channel, reported in the Appendix. This model is used to determine: i) the shapes of the neutron flux and its adjoint, that will be used as weighting functions in the GM model MP-based components; ii) the initial conditions for the GM model MP-based components; iii) the parameters for the solution of the DNP equation. The dependencies of the MP channel model on the stand-alone one are reported in Fig. 4.

The core is described by means of three MP channels, each one acting as an average channel of a particular zone of the core, modelling thermal-hydraulics and DNP balance, as detailed in Section 4.1. The 0-D models that allow to close the fuel loop are those of the reactor plena, the downcomer, the primary Heat Exchanger (HE) and the secondary HE. The corresponding models are presented in Section 4.2. All the components are connected each other in order to build the GM model. Practically, the "thermal-hydraulic connection" is represented by the modelling of the piping. A further comment has to be added concerning core modelling: since each channel is representative of a core region, a suitable description of the overall neutronics has to be determined. That corresponds to determine a "neutronic connection" between the channels. Connections completing the GM model are detailed in Section 4.3.

As far as the equations presented in this section are concerned, the meaning of each symbol is reported in the Nomenclature.

4.1. Multi-physics based core model

The MSRE salt was distributed in 1140 graphite channels that constituted the reactor core. Considering the reactor structure, it is convenient to use the single channel as the fundamental component of the core, thus reducing the geometric complexity of the reactor description. According to this remark, the GM model features a few-channel representation of the core, where each channel is modelled with the MP approach. Actually, thanks to symmetries, only a quarter of the channel has to be modelled. The domain definition is shown in Fig. 5.

With respect to a full MP description, that would include time-dependent coupled neutronics and thermal-hydraulics, some simplifications have been adopted.

As a first simplification, space-dependent neutronics equations are solved during an off-line stage (i.e., with the stand-alone model) and their solution is used in the MP components of the GM model. In practice, the shapes of the solution of the direct and adjoint problem (see the Appendix for details) are used in each of the MP compo-nents, scaled with respect to the power generated in the channel. As shown in Section 4.3, this choice is coherent with the point-kinetics description adopted for the computation of the overall reactor po-wer. As a consequence, the power generated into the channel be-comes an input to the MP components, and acts as the "neutronic connection" in the GM model. Since the solution of the neutron diffusion equations has been obtained on an infinite lattice, the shape of the generated power is the same in each channel, that is not realistic, but is usually considered as an acceptable approximation.

Secondly, as a means to reduce the computational requirements, DNPs are modelled with a single equivalent group approach. When adopting a few group approximation for the neutron precursors, an equivalent decay constant has to be defined, depending on what kind of dynamics is investigated (Hetrick, 1972). In our case, the constant is defined so that the equivalent precursor group can effectively substitute the actual DNP groups in the weighting function for the definition of point-kinetics models (Lapenta et al., 2001), starting from the stand-alone channel solution:

$$F(t) = \int \sum_{i}^{NP} \sum_{n}^{G} \varphi_n^* \lambda_i c_i(t) \chi_{i,n} + (1-\beta) \sum_{n}^{G} \sum_{g}^{G} \varphi_n^* \chi_n \nu_g \Sigma_g^f \varphi_g(t) \mathrm{d}V \tag{1}$$

where the *NP* index is the number of DNP groups and *G* the number of energy groups.

Starting from the definition of the effective DNP fraction in circulating fuel reactors (Mattioda et al., 2000; Aufiero et al., 2014a), and imposing:

$$\begin{cases} \sum_{i}^{NP} c_i = c_{eq} \\ \sum_{i}^{NP} \chi_{i,n} = \chi_{eq,n} \\ \sum_{i}^{NP} \beta_{eff,i} = \beta_{eff} \\ \sum_{i}^{NP} \lambda_i c_i \chi_{i,n} = \lambda_{eq} c_{eq} \chi_{eq,n} \end{cases} \tag{2}$$

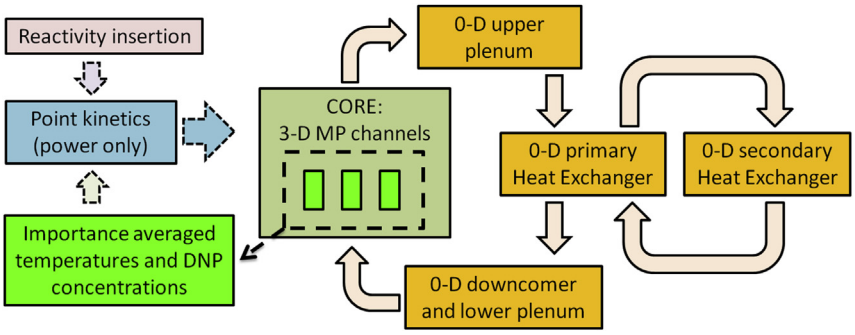

Fig. 3. Conceptual scheme of the Geometric Multiscale model of the MSRE.

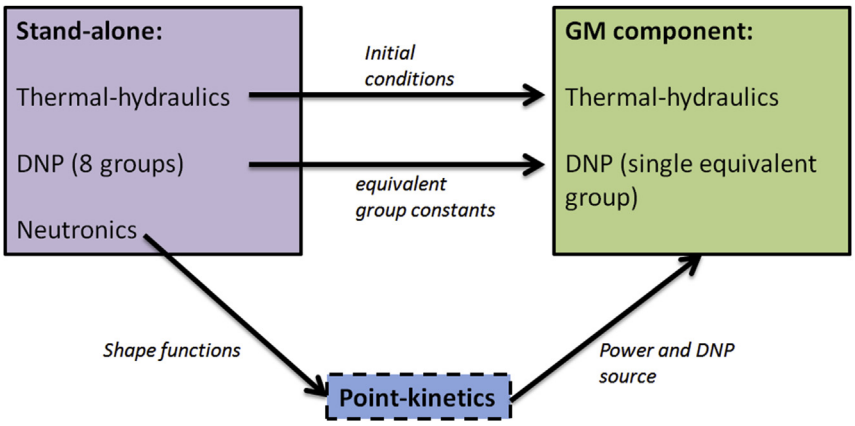

Fig. 4. Dependencies of GM model MP channel component from the stand-alone model.

the following expression of the equivalent decay constant is obtained:

$$\lambda_{eq} = \beta_{eff}\frac{1-\beta}{1-\beta_{eff}}\sum_{n}^{G}\sum_{g}^{G}\int \varphi_n^* \chi_n \nu_g \Sigma_{f,g}\phi_g \,\mathrm{d}V \Big/ \sum_{n}^{G}\int \varphi_n^* c_{eq}\chi_{eq,n}\,\mathrm{d}V \tag{3}$$

Given that the neutron flux shape is imposed and the DNPs are reduced to a single group, the DNP balance equation can be written as:

$$\frac{\partial c_{eq}}{\partial t} + \boldsymbol{u}\cdot\nabla c_{eq} = \beta\frac{Q}{q_0} - \lambda_{eq}c_{eq} \tag{4}$$

where the DNP source is determined from the power source, scaled by a factor q_0, equal to the power released per fission. Symmetry boundary conditions are considered at the surfaces derived from the subdivision of the channel (see Fig. 5), while no flux conditions (homogeneous Neumann boundary conditions) are adopted at the channel wall. "Outflow conditions" (i.e., zero normal gradient) are imposed at the channel outlet. The DNP concentration is fixed at the inlet surface.

Given the above mentioned simplifications, the other coupled physical phenomena considered are: fluid flow (Eqs. (5) and (6)) and heat transfer, modelled with energy conservation equation (Eqs. (7a) and (7b)).

$$\delta\nabla\cdot\boldsymbol{u} = 0 \tag{5}$$

$$\delta\frac{\partial \boldsymbol{u}}{\partial t} + \delta(\boldsymbol{u}\cdot\nabla)\boldsymbol{u} = \nabla\cdot\Big(-p\boldsymbol{I} + \mu\Big((\nabla\boldsymbol{u}) + (\nabla\boldsymbol{u})^T\Big)\Big) - \boldsymbol{g}\delta \tag{6}$$

$$\delta cp\frac{\partial T}{\partial t} + \delta cp\boldsymbol{u}\cdot\nabla T = \nabla\cdot(\boldsymbol{k}\nabla T) + Q \tag{7a}$$

$$\delta cp\frac{\partial T}{\partial t} = \nabla\cdot(\boldsymbol{k}\nabla T) + Q \tag{7b}$$

The flow field in the channel is obtained according to the incompressible form of the Navier–Stokes equations, with Boussinesq approximation for buoyancy effects.

Thermo-physical properties are reported in Table 1. Computing the Reynolds number (equal to 1027.6), the flow regime is determined as laminar. The gravity field **g** is directed along the z axis. Eqs. (5)–(7a) are solved in the fluid domain, while Eq. (7b) is solved

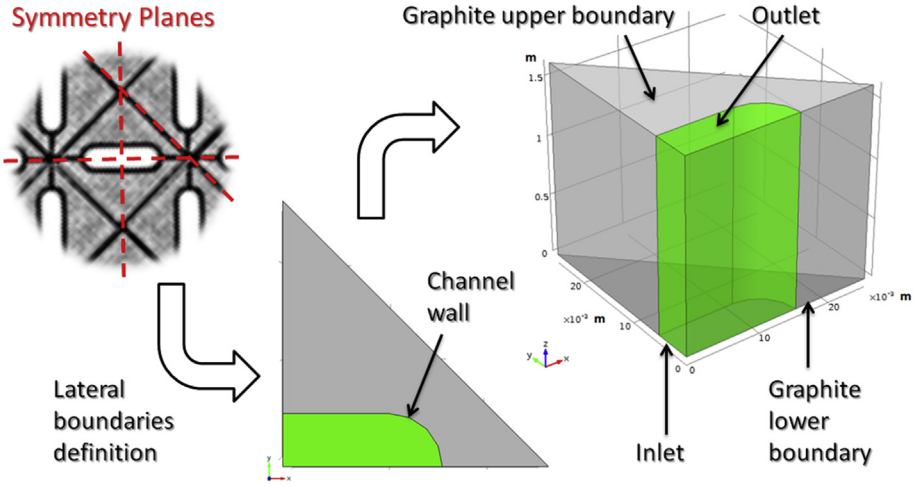

Fig. 5. Geometry of the core channels implemented for MP models. Molten salt and graphite are represented in green and grey, respectively (not in scale). (For interpretation of the references to colour in this figure legend, the reader is referred to the web version of this article.)

Table 1
MSRE thermo-physical properties (Briggs, 1964; Robertson, 1965; Gabbard, 1970; Grimes, 1970; Thoma, 1971; Guymon, 1973).

Core		
Density, salt	2575−0.513·T (°C)	kg m^{-3}
Density, graphite	1874	kg m^{-3}
Thermal conductivity, salt	1.44	W m^{-1} K^{-1}
Thermal conductivity,[a] graphite	53	W m^{-1} K^{-1}
Heat capacity, salt	1983	J kg^{-1} K^{-1}
Heat capacity, graphite	1772	J kg^{-1} K^{-1}
Dynamic viscosity, salt	7.44	mPa s
Primary heat exchanger (hot fluid: core salt; coolant: secondary salt)		
Hot fluid mass flow	168	kg s^{-1}
Coolant fluid mass flow	105	kg s^{-1}
Hot fluid heat capacity	1983	J kg^{-1} K^{-1}
Coolant heat capacity	2146	J kg^{-1} K^{-1}
Hot fluid mass in the heat exchanger	450	kg
Coolant mass in the heat exchanger	170	kg
Heat exchange area	26	m^2
Heat exchange coefficient	3.7	kW m^{-2} K^{-1}
Secondary heat exchanger (hot fluid: secondary salt; coolant: air)		
Hot fluid mass flow	105	kg s^{-1}
Coolant fluid mass flow	75	kg s^{-1}
Hot fluid heat capacity	2146	J kg^{-1} K^{-1}
Coolant heat capacity	1011	J kg^{-1} K^{-1}
Hot fluid mass in the heat exchanger	616	kg
Coolant mass in the heat exchanger	2.4	kg
Heat exchange area	65.6	m^2
Heat exchange coefficient	0.24	kW m^{-2} K^{-1}

[a] In the present work, the graphite is considered isotropic.

in the solid graphite one. The source term in Eq. (7b) is due to heating by gamma radiation and fast neutron slowdown. According to ORNL, 6.3% of the core power is generated into the graphite (Robertson, 1965). For simplicity, the heat source in the graphite is assumed to have the same shape of the power source in the salt, with an appropriate scaling in order to obtain the total power generation determined by ORNL.

Where possible, symmetry boundary conditions are used (as in Fig. 5). No-slip condition is imposed at the channel wall and, in order to simplify the numerical computation, the presence of the hydrodynamic entry length is neglected, hence the flow is considered as fully developed at the channel inlet with a "laminar inlet" weak condition (Comsol, 2012a). At the outlet, a pressure of 1.5 bar (hydrostatic pressure) is imposed with the conditions of no viscous stress (i.e., the right-hand side of Eq. (6) is only dependent on the gravity field). As to the heat transfer, a uniform temperature is imposed at the channel inlet, while "outflow conditions" are considered at the outlet. The top and the bottom of graphite are considered to be thermally insulated.

The above considerations are summarized in Fig. 6. The boundary conditions are further detailed in Section 4.3, in which the connections with the out-of-core components are described.

4.2. Modelling of out-of-core components

The components in the out-of-core part of the plant are the reactor plena with the downcomer and the two heat exchangers. As a modelling choice, these components are represented by 0-D models. Their use is to complete the description of the plant, and to allow determining the boundary conditions for the MP components.

The plena and the downcomer are modelled through the following conservation equations:

$$\sum_k \dot{m}_{k,in}(t) = \dot{m}_{out}(t) \tag{8}$$

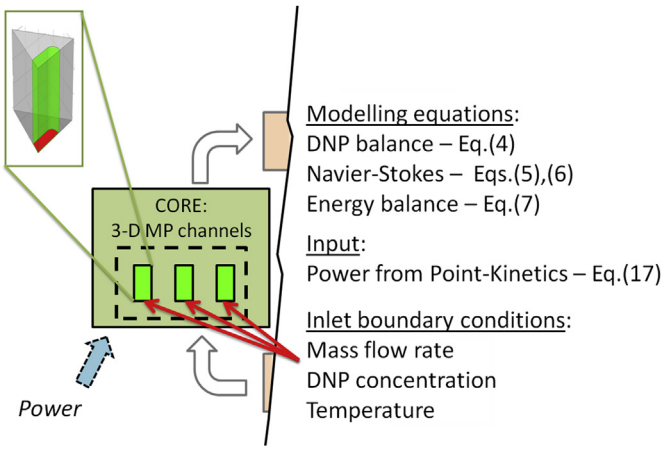

Fig. 6. Conceptual scheme of the core modelling.

$$Mcp_{salt}\frac{\mathrm{d}}{\mathrm{d}t}T_{out}(t) = \left(\sum_k \dot{m}_{k,in}T_{k,in}cp_{salt}\right) - \dot{m}_{out}T_{out}(t)cp_{salt} + Q \tag{9}$$

$$c_{eq,out}(t) = \left(\sum_k \dot{m}_{k,in}c_{eq,k,in}(t)\Big/\sum_k \dot{m}_{k,in}\right) + e^{-\lambda_{eq}t}\int_0^t \frac{\beta}{\Lambda}e^{\lambda_{eq}\vartheta}\frac{(Q(\vartheta)-Q(0))}{q_0}\mathrm{d}\vartheta \tag{10}$$

where $\dot{m}$ is the mass flow rate (the subscript k assumes a value between 1 and 3 in the upper plenum, and is 1 otherwise), M is the mass of salt present in the component, estimated from geometric properties (Robertson, 1965). The plena and the downcomer are low importance parts of the active region. Thus, they can be modelled with a 0-D approach. Nevertheless, a fraction of the reactor power and DNP are there generated. This has been taken into account in Eqs. (8)–(10) with the power source Q.

The primary heat exchanger (salt–salt) is a U-tube type, in which the secondary (coolant) salt flows around the tubes. The secondary heat exchanger (salt-air) is a cross-flow type in which the air-cooled salt flows into the tubes. Both the heat exchangers are modelled with a mean logarithmic temperature approach. Denoting by the subscripts *cd* and *cl* the hot fluid and the coolant, respectively, the salt temperatures are determined from the following equations:

$$\frac{\mathrm{d}T_{cd,out}}{\mathrm{d}t} = -\frac{2}{M_{cd}cp_{cd}}\left(\dot{m}_{cd}cp_{cd}\left(T_{cd,out}-T_{cd,in}\right) + HAh\Delta T_{lm}\right) - \frac{\mathrm{d}T_{cd,in}}{\mathrm{d}t} \tag{11}$$

$$\frac{\mathrm{d}T_{cl,out}}{\mathrm{d}t} = -\frac{2}{M_{cl}cp_{cl}}\left(\dot{m}_{cl}cp_{cl}\left(T_{cl,out}-T_{cl,in}\right) - HAh\Delta T_{lm}\right) - \frac{\mathrm{d}T_{cl,in}}{\mathrm{d}t} \tag{12}$$

$$\Delta T_{lm} = \left(\left(T_{cd,in}-T_{cl,in}\right) - \left(T_{cd,out}-T_{cl,out}\right)\right) \Big/ \ln\frac{\left(T_{cd,in}-T_{cl,in}\right)}{\left(T_{cd,out}-T_{cl,out}\right)} \tag{13}$$

where H is a function of $(T_{cd,in}, T_{cl,in}, T_{cd,out}, T_{cl,out})$ that takes into account the type of the heat exchanger (Bowman et al., 1940). Heat

exchanger properties are reported in Table 1. This table shows the properties in nominal conditions (reactor at full power, 8 MW), the operation point of the HEs at different power being not available. The above considerations are summarized in Fig. 7. The variation of the DNP concentration in the fuel side of the primary HE is taken into account by means of the decay law.

4.3. Connections and boundary conditions

In this sub-section, the connections between the above presented models are described so as to finalize the GM approach. The GM model can be subdivided into two main sections: the core and the cooling loop. The core has been radially subdivided into three zones of equal volume, each one represented by an equivalent 3-D MP channel (see Section 4.1 and Fig. 6). Each channel is representative of the average conditions of the zone. The definition of the three zones and the corresponding fraction of the total generated power (estimated by means of Serpent) is reported in Table 2. The cooling loop is made up of the 0-D modelled components (see Section 4.2 and Fig. 7). The first kind of connection between the different components is the piping, modelled with time-delays. The second kind, herein called "neutronic connection", is determined from a point-kinetics equation, which allows the computation of the reactor power. The different connection types are summarized in Table 3. Taking Figs. 3, 6 and 7 as references, the pipe connections can be identified by the solid line arrows, while the neutronics ones by the dotted line arrows.

From the thermal-hydraulics point of view, each component, be it MP or 0-D, is characterized by an input–output description of three physical variables: energy, mass flow rate, and DNP concentration. Each input is determined from the connections with other components. In particular, energy and DNP transport in the piping is simply modelled as:

$$T_{in,j}(t) = T_{out,j-1}(t - \tau_d) \tag{14a}$$

$$c_{eq,in,j}(t) = c_{eq,out,j-1}(t - \tau_d)e^{-\lambda_{eq}\tau_d} \tag{14b}$$

This means that the quantity passed to the component (j) is determined from the output of component ($j-1$) at time ($t-\tau_d$). The values of time delay adopted for each couple of components are reported in Table 4. On the other hand, since the fluid is incompressible, the mass flow rate changes instantly in each component and no delay is applied to it. For the MP components, the input determines the value of the variables at the inlet surface for boundary condition modelling (see Fig. 6). In this way, the temperature, the DNP concentration and the average fluid ve-locity at the inlet of the channel are updated at each time-step with the values determined from the connection to the lower plenum (0-D component). Concerning the velocity value, it is determined from the mass flow rate coming from the lower plenum and scaled for each channel in order to match the measured distribution of the velocity field at the graphite base, as reported in Kedl (1970).

The "neutronic connection" is obtained using a point-kinetics equation for the determination of the overall reactor power. By employing the point-kinetics theory (Henry, 1958), we consider that the shape of the flux is not going to vary substantially during the transient. Feedback effects are modelled by means of feedback coefficients, in order to be consistent with the use of similar coefficients in the 0-D components. As to the evaluation of the variables needed for the point-kinetics model, we adopted the following average definitions, using the weight function $F(t)$, Eq.(1):

Table 2
Core subdivision: geometric and power generation data.

Component	Core zone equivalent (radial coordinates, cm)	Salt mass, kg	Power fraction, %	Modelling
Hot channel	[7; 41]	513.66	41.78	3-D
Medium channel	[0; 7]∪[41; 57.2]	513.66	30.69	3-D
Peripheral channel	[57.2; 70]	513.66	12.79	3-D
Upper plenum	–	475	3.89	0-D
Lower plenum	–	680	8.59	0-D
Downcomer	–	376	2.26	0-D

Table 3
GM model connections.

Connection type	Variable	Physical connection	Model	Model equations
Hydraulic	Mass flow rate	Pipe	Constant	N. A.
Thermal	Temperature	Pipe	Time delay	Eq. (14a)
DNP	Concentration	Pipe	Time delay	Eq. (14b)
Neutronic	Power	Neutron transport	Point-Kinetics	Eq. (17)

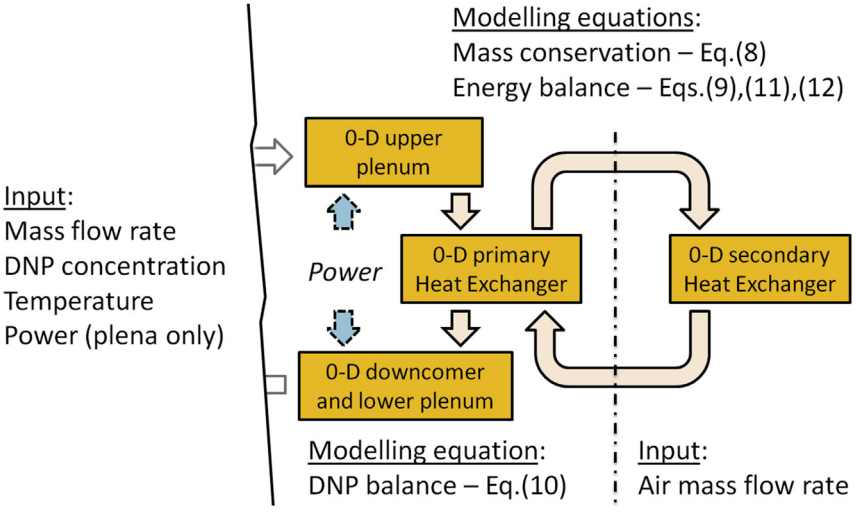

Fig. 7. Conceptual scheme of the cooling loop modelling.

Table 4
Time delay adopted for pipe modelling (Robertson, 1965).

	Model delay, s
Hot leg (upper plenum to HE inlet)[a]	4.7
Cold leg (HE outlet to downcomer)[a]	4.1
Downcomer to lower plenum[a]	1.3
Primary HE outlet to secondary HE inlet	8.24
Secondary HE outlet to primary HE inlet	4.71

[a] Corrected with respect to Robertson (1965), in order to take into account 0-D model time constants.

$$\langle f(\boldsymbol{x},t)\rangle = \frac{\sum_g^G \sum_n^G \int \varphi_n^*(\boldsymbol{x}) f(\boldsymbol{x},t) \varphi_g(\boldsymbol{x}) dV}{F(t)} \tag{15}$$

for the temperature and

$$\langle f(\boldsymbol{x},t)\rangle = \frac{\sum_n^G \int \varphi_n^*(\boldsymbol{x}) f(\boldsymbol{x},t) \mathrm{d}V}{\Lambda F(t)} \tag{16}$$

for the precursor term. In Eqs. (15) and (16), the term $\varphi_n^*(\boldsymbol{x})$ is the adjoint flux for the stand-alone stationary problem (as described in the Appendix), or the importance function. Both the direct flux and the adjoint flux shapes are taken as fixed, as described in Section 4.1. The shapes are reported in Fig. 8. For the 0-D components, the average is implicitly defined equal to the state variable.

Thus, collecting the required averages from the MP components, the reactor power can be determined and used as an amplitude factor to be multiplied by the shape of the source term in Eqs. (4), (7), (9) and (10). This is described by:

$$\frac{\mathrm{d}P}{\mathrm{d}t} = \frac{P}{\Lambda}\left(\rho_{IN} - \beta_{eff} + \sum_j \alpha_{T,j}\left(\langle T_j(\boldsymbol{x},t)\rangle - \langle T_j(\boldsymbol{x},0)\rangle\right)\right) + \lambda_{eq}\langle c_{eq}(\boldsymbol{x},t)\rangle \tag{17}$$

$$Q_j(\boldsymbol{x}) = P q_{f,j} shape(\boldsymbol{x}) \tag{18}$$

The considered components (represented by index j) are the MP channels, the plena and the downcomer, while the zone power factor q_f is the ratio of the power generated into the component j to the total reactor power. The zone power factor has been determined by means of a Serpent based model (Zanetti et al., 2014) of the reactor. Its values are reported in Table 2 for the different components. The power shape function is determined by a combination of the flux shapes (Fig. 8) in each channel, while it is unitary in the 0-D components (see the Appendix for details).

The neutronic parameters are summarized in Tables 5 and 6, as determined by Serpent. In particular, the temperature reactivity coefficients are computed as:

$$\alpha_{T,j} = -\frac{1}{k_{eff}}\frac{\Delta k_{eff}}{\Delta T_j} \tag{19}$$

taking into account the Doppler effect, the density variation and the graphite expansion, as described in Zanetti et al. (2014). The effective delayed neutron fraction β_{eff}(Mattioda et al., 2000; Aufiero et al., 2014a) and the equivalent decay constant λ_{eq} (Eq.(3)) have been computed by means of the stand-alone model, which takes into account fuel motion effects. In particular, β_{eff} and λ_{eq} were computed equal to 149.15 pcm and 0.0702 s^{-1}, respec-tively. The β_{eff} determined with the fuel in motion differs from the one with static fuel, reported in Table 5, for different reasons: i) the production of delayed neutrons in the out-of-core part of the pri-mary circuit, where their importance is very low, or null; ii) the distortion of the DNP distribution in the core with respect to the static case, with the relocation of the maximum of the distribution towards the core exit, where the importance is lower (and the escape probability is higher). The difference between the static and moving fuel β_{eff} can be represented by a loss of reactivity ($-\rho_0$). This loss requires a compensation in order to allow steady-state condition. The values of $-\rho_0$ predicted by the stand-alone model, as well as the contribution of each DNP group to the total reactivity loss, are shown in Table 7. The main contribution to $-\rho_0$ is due to the DNP groups characterized by lower decay constant (groups 1–5), while the other groups mainly decay into the core.

4.4. Numerical solution

The MP model has been solved using the finite element software COMSOL® Multiphysics (Comsol, 2012a). The geometry has been meshed so as to achieve a good compromise between

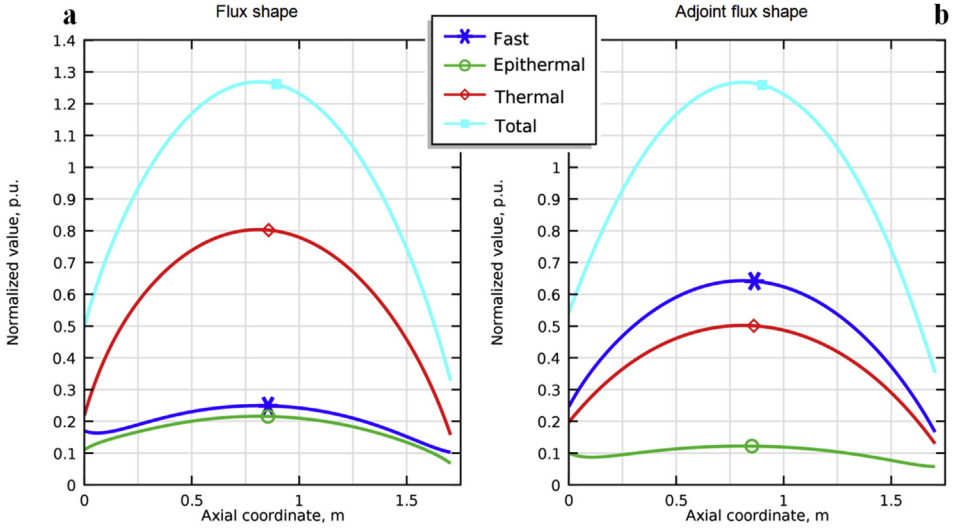

Fig. 8. Flux shapes on the z axis as computed by the stationary model: (a) forward problem solution; (b) adjoint problem solution. Values normalized to the average value of the total flux. Energy bounds: thermal group, from 0 to 2 eV; epithermal group, from 2 eV to 1 keV; fast group, above 1 keV.

Table 5
MSRE neutronic data, computed by means of Serpent for static fuel.

Delayed neutron precursors properties									
Group	1	2	3	4	5	6	7	8	Total
λ_i, 1/s	0.012	0.028	0.043	0.133	0.292	0.666	1.635	3.555	–
β_i, pcm	22.075	45.478	39.590	56.213	83.461	10.817	16.599	3.189	277.427
St. Dev, %	1.084	0.75	0.797	0.684	0.57	1.557	1.271	2.892	0.308
Λ, *s*									$3.54 \cdot 10^{-4}$
St. Dev, %									0.019

Table 6
MSRE reactivity feedback coefficients, computed by means of Serpent.

	Total	Graphite	Salt				
			All	Core	Downcomer	Lower plenum	Upper plenum
α_T, pcm/K	−17.64	−4.5	−13.64	−11.97	−0.35	−1.01	−0.84
St. Dev, %	0.41	1.6	0.56	0.6	19.6	6.7	8.2
α_V, pcm/%	−608.47						
St. Dev, %	0.63						

Table 7
Reactivity loss ($-\rho_0$) due to DNP recirculation.

Group	1	2	3	4	5	6	7	8	Total
$-\rho_0$, pcm	13.39	26.47	24.37	30.13	31.063	1.882	0.922	0.055	128.28
$-\rho_0/\beta_i$, %	60.66	58.20	61.56	53.60	37.22	17.40	5.55	1.72	46.24

numerical accuracy and computational requirements. The mesh consists in 28,320 elements obtained from the extrusion of the 2-D mesh of the channel base. Different spacing has been used in the solid and the fluid region during extrusion. Detail of the upper part of the mesh is portrayed in Fig. 9. In the view of a full reactor model, if the same meshing approach was used for all the reactor channels, the mesh would consist in more than $127 \cdot 10^6$ elements, that would lead to an extremely computational inten-sive model.

For solution, the chosen elements are Lagrangian and first-order. To further reduce the computational cost (memory requirements) of the simulation, the segregated solver has been adopted (Comsol, 2012b). The MP model equations have been solved adopting the direct solver MUMPS method for the solution of each segregated group.

All the other models (0-D and point-kinetics) have been implemented in MATLAB® Simulink (Matlab, 2012) and solved with the *Ode15s* solver. In Simulink, equations or parts of equations are organized into "blocks". Each block contains a cluster of instructions for the program, and is connected to the other ones in order to transfer state variable values. The MP models are integrated in Simulink with commands written in S-Function blocks (Matlab, 2012).

Since the MSRE plant model is implemented in Simulink, this environment acts as "master", whereas COMSOL acts as "slave", meaning that the main simulation is carried on by Simulink, and COMSOL is used when required to provide the values processed by Simulink. A scheme of the main operations performed by Simulink and COMSOL is depicted in Fig. 10. At the beginning of the solution procedure, the program identifies the block dependencies and the solution order. In general, the main conceptual solution stages at each time-step can be summarized as follows: i) ODEs are solved in Simulink. ii) The boundary conditions of the MP models, dependent on the 0-D components, are updated with current Simulink values. iii) The COMSOL transient solver is called to simulate the evolution of the MP model state variables for a length equal to the Simulink time-step, imposing as initial condition the solution at the previous time-step. iv) Quantities such as the average DNP concentration and temperatures are gathered from COMSOL and stored in Simulink. v) When all blocks have been processed, Simulink determines if the variation of the state variables is compatible with the imposed tolerance; if not, the solution procedure is repeated for the current time-step, until the convergence criterion is satisfied (if necessary, the length of the current time-step is reduced). vi) When the convergence criteria are met, the procedure is repeated for a new time-step. Thanks to the Simulink time-dependent solver, a semi-implicit scheme is used for the connection of the two codes. From the MP model perspective, the whole simulation consists in a series of subsequent small transients with the boundary conditions changed at the beginning of each transient.

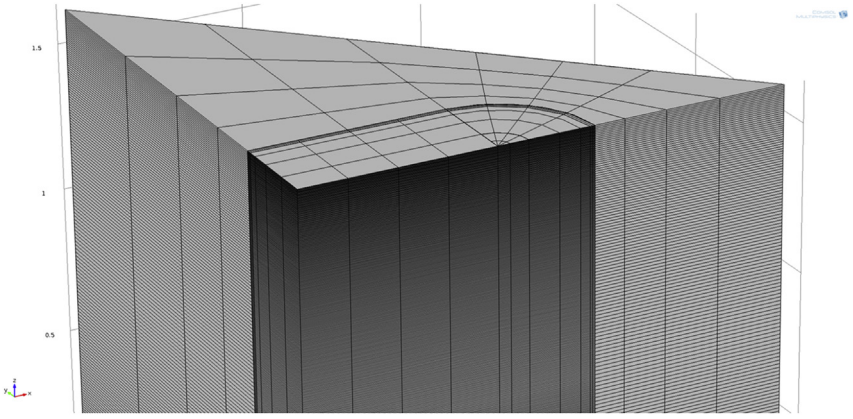

Fig. 9. Detail of the mesh of the MP channel (not in scale).

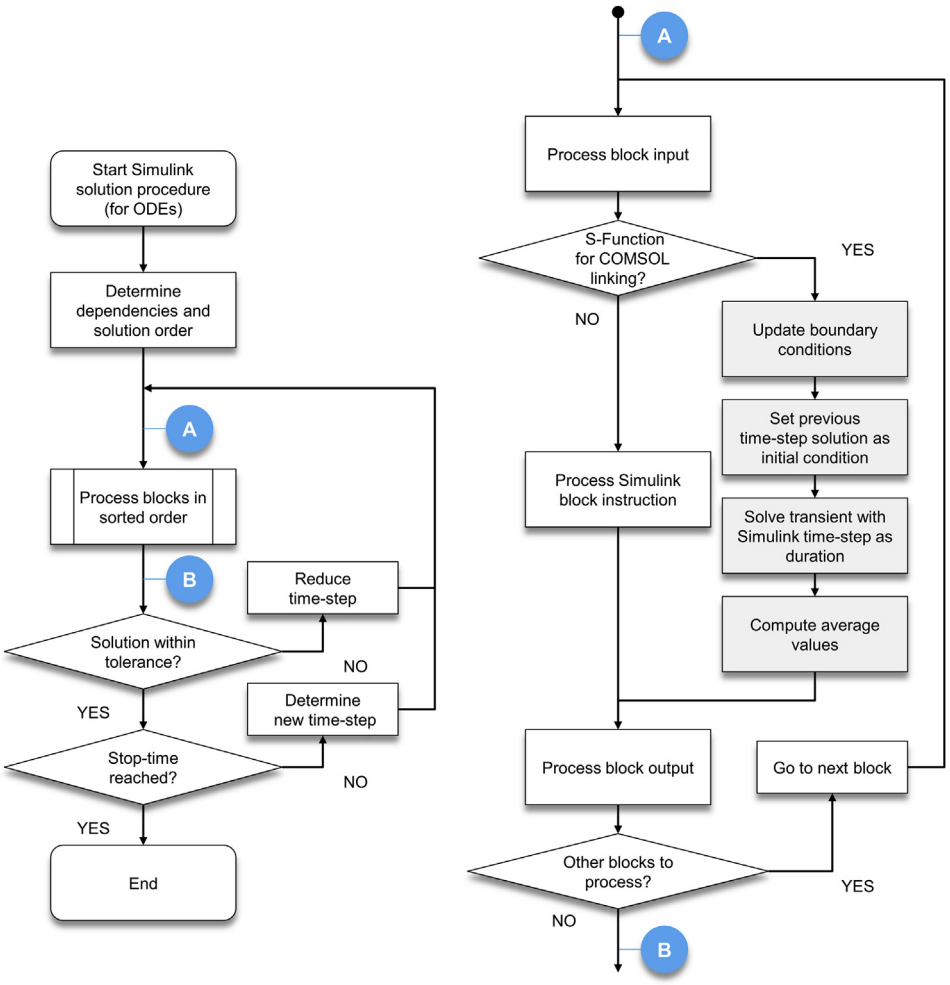

Fig. 10. Conceptual scheme of Simulink–COMSOL solution stages (white stages and grey stages are performed by Simulink and COMSOL, respectively).

5. Results and discussion

In this section, the results obtained by applying the GM approach to the MSRE plant are discussed. The model includes all the key components necessary to catch the dynamic behaviour of the plant (i.e., core channels, plena, loop pipes, heat exchangers), and describes neutronics, DNP drift and heat transfer. The analysis is focused on the dynamic behaviour, in order to provide an assessment of the GM approach for MSR dynamics. Thus, the results are compared to available experimental data (Steffy, 1970a), both in time and frequency domain.

The first reproduced transient (Fig. 11) is the response of the MSRE at 8 MW to a total insertion of 13 pcm, with a rate of 5.3 pcm/s. Nominal plant operation conditions are considered. The simulation time was restricted to the available data points, but the thermal transient of both salt and graphite is not extinguished in such time interval. The heat exchange system is set to dissipate 8 MW during the whole transient.

The second reproduced transient (Fig. 12) is the response of the MSRE at 5 MW to a total insertion of 19 pcm, obtained in two steps with a rate of 5.3 pcm/s. The operating conditions in the HEs and the secondary circuit are not reported in the reference (Steffy, 1970a). For the purpose of simulation, two cases have been considered: i) in the first one (here below referred to as case A), the stationary fuel outlet temperature from the primary heat exchanger is set equal to the one at 8 MW, the air temperature at the inlet of the secondary HE is fixed at 35 °C, and the heat exchange system is set to dissipate 5 MW during the whole transient; ii) in the second one (case B), the same transient has been run fixing the temperature at the inlet of the primary HE, neglecting the recirculation effects in the secondary circuit.

5.1. Time domain assessment

The trends of power and of the importance-averaged salt and graphite temperatures are reported in Fig. 11 for the 8 MW case and in Fig.12 for the 5 MWone. Temperatures are given as difference with respect to the initial condition. The overall behaviour shown in Figs.11 and 12 can be explained as follows. The initial power increase due to the reactivity step is balanced in few seconds by the negative temperature feedback. This feedback causes a steep decrease, after which the power undergoes a plateau until the hot salt generated during the power peak re-enters the core. When this happens (starting from about 16.5 s), the temperature feedbacks lead to another sudden decrease in the power, which then smoothly reaches a steady-state value featured by average salt and graphite temper-atures high enough to counterbalance the initial reactivity insertion. Due to the large feedback coefficients, the DNP recirculation effects are difficult to individuate during MSRE power-range transients.

In the simulations, the first plateau is not well defined because of the effects of the thermal behaviour of the graphite. It was shown by Cammi et al. (2012) that graphite in stationary conditions is cooled

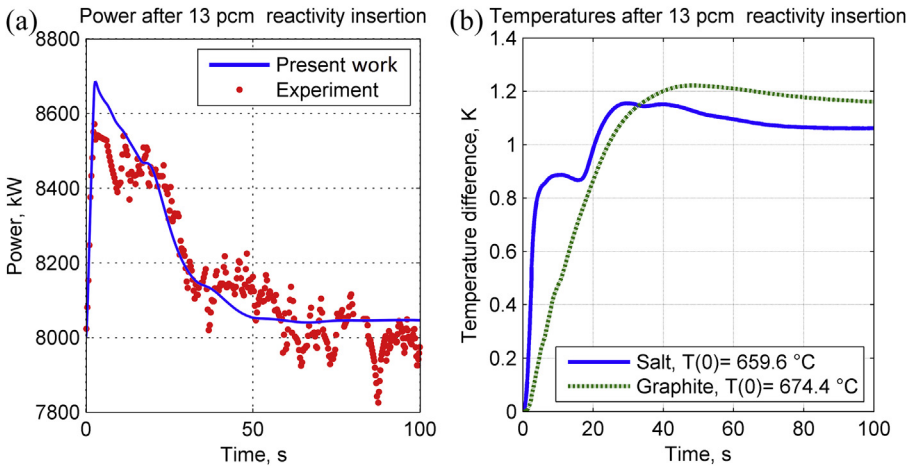

Fig. 11. MSRE reactivity insertion transient at 8 MW: (a) power; (b) temperatures.

by the fluid fuel, whereas it is heated by the fuel during the rise of power, due to the local increase of the salt temperature above the graphite one, with the outcome of an inversion of the heat flux. As a consequence, the rise of the graphite temperature is fast enough to introduce an unbalanced reactivity effect, that results in a slow reduction of the power where the plateau is expected.

The comparison with the experimental data shown in Figs. 11a and 12a points out an acceptable agreement. The discrepancy found in the 5 MW transient (Fig. 12a) after 40 s (when the fuel comes back into the core the second time – see Fig. 12b) is related to the definition of the HEs operating point (as mentioned, not indicated in the ORNL report), which mainly influences the second part of the transient. It is worth noting that the model tracks the experimental data with very good accuracy during the first part of the simulated transient in both the considered cases A and B.

The high noise in the experimental data is due to the presence of helium bubbles in the core, affecting the salt density (Steffy, 1970a). Considering the void coefficient (see Table 6), it is sufficient a disturbance of ±0.20% in the overall quantity of void in the core to produce oscillations of ±1.25 pcm, that is compatible with the amplitude of the registered power oscillations. To check this effect, by adopting the 0-D model developed in Cammi et al. (2012), we excited the system with an oscillating reactivity input (fundamental at 1 rad/s and upper harmonic at 2 rad/s) with an amplitude of 2.5 pcm. The effect on the reactor power is then compared with a portion of the experimental power measurement in Fig. 13, showing the compatibility between the registered power behaviour and the supposed void effect.

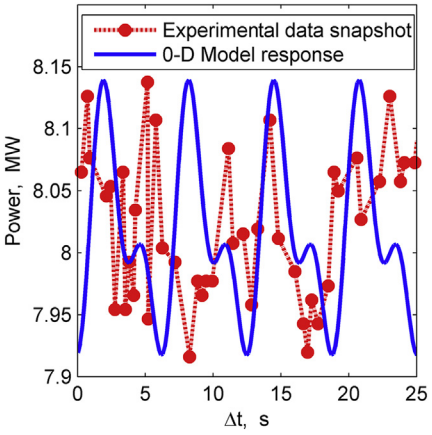

Fig. 13. Test of the effects of reactivity oscillation due to voids (0-D model).

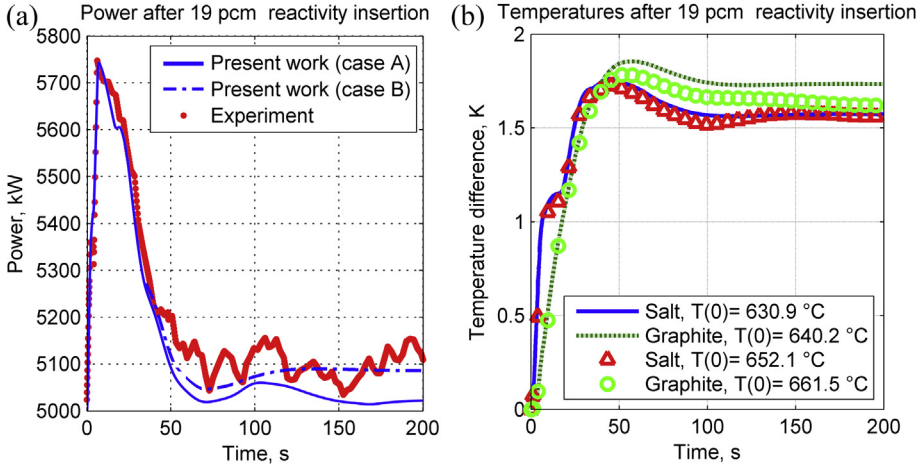

Fig. 12. MSRE reactivity insertion transient at 5 MW: (a) power; (b) temperatures, with the lines representing the case A and the marks the case B.

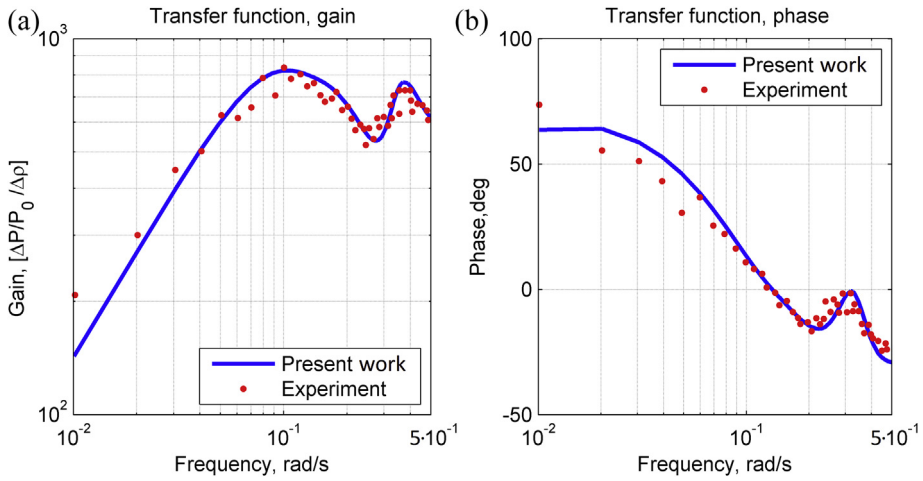

Fig. 14. MSRE power/reactivity transfer function at 8 MW: (a) gain; (b) phase.

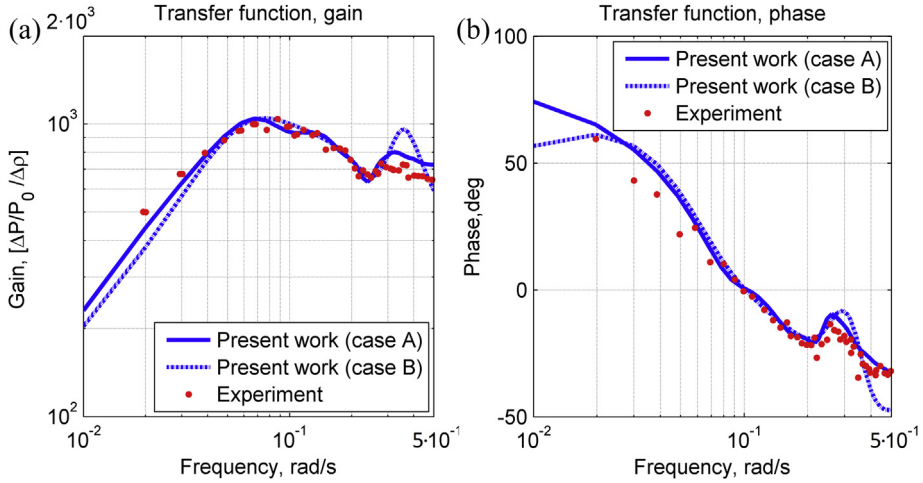

Fig. 15. MSRE power/reactivity transfer function at 5 MW: (a) gain; (b) phase.

5.2. Frequency domain assessment

A better insight in the model accuracy can be attained from a frequency domain analysis on the basis of the transfer function measurements performed during MSRE operation. In particular, three different approaches were adopted by ORNL (Steffy, 1970a,b) for transfer function experimental measurements, giving comparable results. Among the aforementioned approaches, Samulon's method (Samulon, 1951) is based on system response to a known signal, typically a step. For that reason, Samulon's method was also adopted for the determination of the GM model transfer function. The results are reported in Fig. 14 for the 8 MW case, and in Fig. 15 for the 5 MW one.

The measurement of the transfer function is of great interest, because it gives information over a large part of the dynamical range of the reactor. Therefore, the comparison of the transfer function of the model with the experimental one allows a sound assessment of the model predictive capabilities with respect to the behaviour of the reactor.

As can be noted in Figs. 14 and 15, the frequency responses are characterized by a dip in the amplitude diagram at a frequency of about 0.25 rad/s, which results from temperature feedbacks originated by the salt re-entering the core (the circulation time in the primary circuit is about 25 s, and can be subdivided in 8.5 s for the core region and 16.5 for the external loop). In fact, during a periodic reactivity perturbation at 0.25 rad/s, the fuel heated in the core returns to it exactly one period later, thus causing a reactivity feedback effect that overlaps with the externally-imposed perturbation. This effect is still present, but reduced, after another recirculation period (0.0125 rad/s). This is less appreciable due to the scattering in the experimental data and the model damping in the simulated ones (due to the averaging procedure in the 0-D modelling, that includes point-kinetics). The reactor shows a more dumped behaviour as the power level increases. This feature is in agreement with the time domain data and can be evinced from the amplitude diagram, which shows that the relative power change is smaller at higher power levels.

The results of simulations are in a good agreement with the experimental data,[2] both in the case at 8 MW and at 5 MW. Concerning the 5 MW case (see Fig. 15), the transfer function obtained fixing the HE inlet temperature is also compared with experimental data, showing that the results are not completely compatible. This indicates that the effect of the secondary circuit on the reactor behaviour cannot be modelled by a simplified energy balance, but the dynamics of the whole HE system has to be taken into account.

[2] The available experimental data (Steffy, 1970a) have been limited to the ones considered reliable by the measurement team (Steffy, 1970b).

6. Conclusions

In this work, the Geometric Multiscale (GM) approach is presented as a means to reduce complexity and computational requirements of the Multi-Physics Modelling (MPM) for Molten Salt Reactors (MSR). A GM model for the Molten Salt Reactor Experiment (MSRE) dynamics has been developed, and assessed on the basis of the available experimental data for reactivity induced power-range transients, showing satisfactory predicting capabilities both in time and frequency domain. The good results obtained in the frequency domain are of particular interest because they give information over a large part of the dynamic range of the system, thus allowing a more sound assessment of the model predictive capabilities than the direct comparison with few time-domain sets of data.

More in detail, from the presented work the following concluding remarks can be drawn.

i) The attention has been focused on the MSRE due to the availability of detailed design and experimental data, developing a dedicated GM model. However, the same modelling approach can be applied to other concepts of graphite-moderated MSRs, such as the recent reactor configurations proposed by Furukawa et al. (2008), LeBlanc (2010) and the Chinese National Energy Administration (Serp et al., 2014). Actually, the good results obtained with the GM MSRE model give a clear indication that the GM approach can be fruitfully used to prepare compact MP-based MSR models.

ii) In order to simulate the overall plant dynamics of the MSRE without over-detailing the system characterization, the GM model has been implemented taking advantage of the coupling between COMSOL Multiphysics and MATLAB Simulink. The proposed implementation considers a simplified MP description of the reactor core, in which heat transport, DNP convection, and fluid-dynamics are solved for three D channels representing different core zones. Neutronic modelling is based on a point-kinetics-like approach. The boundary conditions of the MP channel models are handled by 0-D models of the cooling loop components (reactor plena, downcomer, heat exchangers). Thus, the components considered to be more important are modelled with a higher level of detail. The model can be used to simulate reactivity insertions, changes in the mass flow rate and power transients. We limited the simulations to transients comparable with the available experimental data in the power-range. It is worth noting that the GM approach is very flexible (thanks also to the native interface-ability of COMSOL with MATLAB), and this feature can be suitably exploited by adjusting the level of refinement or simplification of the adopted models according to the specific needs of analysis.

iii) The presented GM model, although very simplified, is sufficient to correctly reproduce the reactor neutronic behaviour for reactivity insertions. In particular, the use of point-kinetics equation, with importance-weighted temperatures and DNP concentration, turned out to be adequate for predicting the reactor dynamic behaviour. Actually, neutronics was the most simplified physics, since a single DNP group and fixed flux shapes (equal for each channel) were used. In principle, neutron diffusion equations may be solved during on-line computation using suitable albedo conditions as neutronic connections to enhance accuracy. Also, more than one DNP group can be used. However, computational requirement would increase.

iv) The benefits of the adoption of the GM approach should be sought in comparison with the MPM one. In general, the MPM approach is highly valued for the accuracy that it offers when modelling concurrent physical phenomena that are of interest in a nuclear reactor. However, the computational costs of the MPM approach are not considered to be sustainable when dealing with very complex structures and/or large geometries. The GM approach allows reaching a good compromise between the computational complexity and the accuracy of the system description, reducing the constraints on the dimensional description and enhancing modularity and flexibility of model formulation, with the possibility of studying also control-oriented applications. Such applications can exploit the capabilities of the Simulink environment, and will be the subject of future developments of the presented GM approach.

Acknowledgements

Authors express their gratitude to Dr. Claudia Guerrieri (Politecnico di Milano) for the fruitful discussions and criticism. The authors would also like to acknowledge the reviewers, who gave useful suggestions for improving the manuscript.

Appendix

This Appendix describes the stand-alone channel model used to compute stationary properties for the implementation of the GM model.

In order to adopt consistent boundary conditions, it is necessary to consider an expanded computational domain with respect to the domain presented for the MP channel components of the GM model (Fig. 5). In particular, a rough representation of the plena salt is used in the stand-alone model. The domain definition is shown in Fig. A.1. Each plenum domain volume was determined so as to obtain within it a power density compatible with the one determined with the Serpent model (Zanetti et al., 2014).

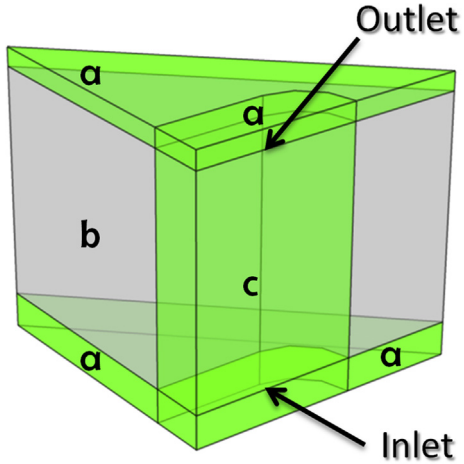

Fig. A.1. Geometry of the stand-alone channel model of the core (not in scale). The different region are defined as: (a) plena domain; (b) graphite domain; (c) salt domain.

Different coupled physical phenomena are considered: laminar fluid flow, Eqs. (A.1) and (A.2); heat transfer, Eq. (A.3); DNP advection, Eq. (A.4); neutron transport, Eq. (A.5), with diffusion approximation (Bell and Glasstone, 1970).

$$\delta \nabla \cdot \boldsymbol{u} = 0 \tag{A.1}$$

$$\delta(\boldsymbol{u}\cdot\nabla)\boldsymbol{u} - \nabla\cdot\Big(-p\boldsymbol{I} + \mu\Big((\nabla\boldsymbol{u}) + (\nabla\boldsymbol{u})^T\Big)\Big) = -\boldsymbol{g}\delta \tag{A.2}$$

$$\delta cp\boldsymbol{u}\cdot\nabla T - \nabla\cdot(\boldsymbol{k}\nabla T) = Q \tag{A.3a}$$

$$-\nabla\cdot(\boldsymbol{k}\nabla T) = Q \tag{A.3b}$$

$$\boldsymbol{u}\nabla c_i + \lambda_i c_i = \beta_i \sum_g^G \upsilon_g \Sigma_g^f \varphi_g \quad \text{for } i = 1,\ldots,NP \tag{A.4}$$

$$\nabla\cdot\left(D_g\nabla\varphi_g\right) - \Sigma_g^R\varphi_g + (1-\beta)\chi_g\sum_n^G \upsilon_n\Sigma_n^f\varphi_n + \sum_{n\neq g}^G \Sigma_{n\to g}^S\varphi_n = -\sum_i^{NP}\chi_{i,g}\lambda_i c_i \quad \text{for } g = 1,\ldots,G \tag{A.5}$$

The meaning of each symbol is reported in the Nomenclature. Eqs. (A.1)–(A.3) are used in the MP channel components of the GM model. The geometric domains and the treatment of the boundary conditions are the same described in Section 4.1 for Eqs. (5)–(7). The heat source in the salt domain is determined as:

$$Q(\boldsymbol{x}) = \sum_g^G \varepsilon\Sigma_g^f\varphi_g(\boldsymbol{x}) \tag{A.6}$$

where $\varepsilon\Sigma_g^f$ is the product of the energy released per fission by the macroscopic fission cross-section for the gth energy group of neutrons. The heat source (gamma radiation and fast neutron slowdown) in Eq. (A.3a) is determined as described in Section 4.1. From Eq. (A.6), the following definition of the power shape function in the MP components is obtained:

$$shape(\boldsymbol{x}) = \sum_g^G \frac{\varepsilon\Sigma_g^f\varphi_g(\boldsymbol{x})\int_{Salt}\mathrm{d}V}{\int_{Salt}\varphi_g(\boldsymbol{x})\mathrm{d}V} \Big/ \int_{Salt} Q(\boldsymbol{x})\,\mathrm{d}V \tag{A.7}$$

Eq. (A.4) is solved in the salt domain. Eight groups of precursors are considered. DNP drift has been taken into account through the introduction of a convective term. Symmetry boundary conditions are considered where possible, while homogeneous Neumann boundary conditions are adopted at the channel wall. "Outflow conditions" are imposed at the channel outlet. The following condition is imposed at the inlet (see Fig. A.1):

$$c_i(\boldsymbol{x}) = e^{-\lambda_i\tau_c}\int_{Outlet} c_i(\boldsymbol{x})\mathrm{d}A \Big/ \int_{Outlet}\mathrm{d}A \tag{A.8}$$

where τ_c is the circulation time in the out-of-core part of the loop. In the plena domain, the DNP concentration is assumed uniform – roughly simulating mixing – and its value is set equal to the one at the respective salt domain boundary.

Finally, Eq. (A.5) is solved in each domain. The modelling of the spatial distribution of the neutron flux is based on the diffusion theory, considering the following three energy groups: i) fast group, above 1 keV; ii) epithermal group, from 1 keV to 2 eV; and iii) thermal group, from 2 eV to 0. The cross-sections adopted in the model, as well as the other neutronic parameters (assumed constant) have been generated by the Monte Carlo code Serpent/PSG2 (Leppänen, 2007) – see Table A.1. For the details of the model, we refer to (Zanetti et al., 2014). Where possible, symmetry boundary conditions are used. The neutron flux is set equal to zero at the top face of the upper plenum domain and at the bottom face of the lower plenum domain. The DNP concentration is set equal to zero in the graphite domain. Since symmetry conditions are imposed at the lateral boundaries, an infinite lattice configuration is assumed.

Table A.1
Neutronic constants used for neutron diffusion solution. Energy groups: 1) fast group, above 1 keV; 2) epithermal group, from 1 keV to 2 eV; 3) thermal group, from 2 to 0 eV.

Symbol	Salt[a]	Graphite[a]	Unit
D_1	1.203 10^{-2}	1.096 10^{-2}	m
D_2	1.185 10^{-2}	0.793 10^{-2}	m
D_3	1.129 10^{-2}	0.760 10^{-2}	m
Σ_1^R	0.52	0.83	m^{-1}
Σ_2^R	0.94	1.01	m^{-1}
Σ_3^R	1.16	0.04	m^{-1}
Σ_1^f	0.01	0.00	m^{-1}
Σ_2^f	0.24	0.00	m^{-1}
Σ_3^f	0.96	0.00	m^{-1}
$\Sigma_{1\to2}^S$	0.60	1.01	m^{-1}
$\Sigma_{1\to3}^S$	0.00	0.00	m^{-1}
$\Sigma_{2\to1}^S$	0.01	0.02	m^{-1}
$\Sigma_{2\to3}^S$	0.48	0.83	m^{-1}
$\Sigma_{3\to1}^S$	0.00	0.00	m^{-1}
$\Sigma_{3\to2}^S$	0.00	0.00	m^{-1}
υ_1	2.526	0.000	–
υ_2	2.488	0.000	–
υ_3	2.487	0.000	–
χ_1	1.00	0.00	–
χ_2	0.00	0.00	–
χ_3	0.00	0.00	–
$\chi_{i,1}$	0.125	0.00	–
$\chi_{i,2}$	0.00	0.00	–
$\chi_{i,3}$	0.00	0.00	–

[a] Since the cross-sections generated by Serpent have a statistical uncertainty, the adopted values have been truncated above the uncertain digit.

The adjoint problem has been also implemented, and was formulated according to Lapenta and Ravetto (2000), to which we refer for further details. In short, the following equations have been considered:

$$-\boldsymbol{u}\nabla c_i^* + \lambda_i c_i^* = \lambda_i\sum_g^G \chi_{i,g}\varphi_g^* \quad \text{for } i = 1,\ldots,NP \tag{A.9}$$

$$\nabla\cdot\left(D_g\nabla\varphi_g^*\right) - \Sigma_g^R\varphi_g^* + (1-\beta)\chi_g\sum_n^G \upsilon_n\Sigma_n^f\varphi_g^* + \sum_{n\neq g}^G \Sigma_{n\to g}^S\varphi_g^* = -\upsilon_g\Sigma_g^f\sum_i^{NP}\beta_i c_i^* \quad \text{for } g = 1,\ldots,G \tag{A.10}$$

Eq. (A.9) is solved in the salt domain only. The boundary conditions are determined in the same manner used for Eq. (A.4), with the following distinctions: i) "outflow conditions" are imposed at the channel inlet; ii) the following condition is imposed at the outlet (see Fig. A.1):

$$c_i^*(\boldsymbol{x}) = e^{\lambda_i \tau_c} \int_{Inlet} c_i^*(\boldsymbol{x}) \mathrm{d}A \Big/ \int_{Inlet} \mathrm{d}A \tag{A.11}$$

The adjoint DNP concentration in the plena region is assumed constant, like the DNP concentration in the forward problem.

Eq. (A.10) is handled as Eq. (A.5).

Acronyms

ARE	Aircraft Reactor Experiment
DNP	Delayed Neutron Precursor
GM	Geometric Multiscale
HE	Heat Exchanger
MP	Multi-Physics
MPM	Multi-Physics Modelling
MSBR	Molten Salt Breeder Reactor
MSR	Molten Salt Reactor
MSRE	Molten Salt Reactor Experiment
ODE	Ordinary Differential Equation
ORNL	Oak Ridge National Laboratory
PDE	Partial Differential Equation
p.u.	per-unit: normalized quantity
0-D, 3-D	Zero-, Three-Dimensional

Nomenclature

Latin symbols

A	area, m^2
c	DNP concentration, m^{-3}
c^*	adjoint DNP concentration, −
cp	specific heat, J kg^{-1} K^{-1}
D	neutron diffusion coefficient, m
f	generic function
F	weight function
$\boldsymbol{g}$	gravity field, m s^{-2}
G	number of neutron energy groups for multi-group diffusion
h	heat exchange coefficient, kW m^{-2} K^{-1}
H	heat exchanger function
$\boldsymbol{k}$	thermal conductivity, W m^{-1} K^{-1}
k_{eff}	effective multiplication factor
M	mass, kg
NP	number of DNPs
$\dot{m}$	mass flow rate, kg s^{-1}
p	pressure, bar
P	power, W
P_0	reference power, W
pcm	per cent mille ($=10^{-5}$)
Q	volumetric heat source, W m^{-3}
q_f	zone power factor, −
q_0	scale factor, J
t	time, s
T	temperature, K
u, $\boldsymbol{u}$	salt velocity, m s^{-1}
V	volume, m^3
$\boldsymbol{x}$	system coordinate vector $\mathbf{x} = (x, y, z)$ in the 3-D geometry

Greek symbols

α	reactivity coefficient
β	DNP total fraction, −
β_i	DNP fraction of the ith precursor group, −
β_{eff}	effective DNP fraction, −
γ	fraction of power released in the salt, −
δ	density, kg m^{-3}
ΔT_{lm}	log mean temperature difference, K
ε	average energy released per fission, J
ϑ	time auxiliary variable
λ	decay constant, s^{-1}
Λ	mean neutron generation time, s
μ	dynamic viscosity, mPa s
υ	average number of neutrons per fission, −
ρ	reactivity, −
ρ_{IN}	reactivity insertion through control rods, −
ρ_0	reactivity variation from steady-state condition due to DNP circulation, −
Σ	macroscopic cross-section, m^{-1}
τ_d	time delay, s
τ_c	out-of-core circulation time, s
φ	neutron flux, m^{-2} s^{-1}
φ^*	adjoint neutron flux, −
χ	fission spectrum, −

Subscripts/superscripts

$(-)_{cd}$	cooled fluid in heat exchanger
$(-)_{cl}$	coolant fluid in heat exchanger
$(-)_{eq}$	single equivalent DNP group
$(-)_g$	neutron energy group g
$(-)_i$	DNP group index
$(-)_{in}$	inlet
$(-)_j$	GM model component index
$(-)_k$	index of inlet in GM components
$(-)_n$	neutron energy group n
$(-)_{n\to g}$	from neutron group n to neutron group g
$(-)_{out}$	outlet
$(-)_T$	temperature
$(-)_V$	void
$(-)^*$	adjoint
$(-)^f$	fission
$(-)^R$	removal
$(-)^s$	scattering

Other symbols

$\langle\rangle$	average value

References

Aufiero, M., Brovchenko, M., Cammi, A., Clifford, I., Geoffroy, O., Heuer, H., Laureau, A., Losa, M., Luzzi, L., Merle-Lucotte, E., Ricotti, M., Rouch, H., 2014a. Calculating the effective delayed neutron fraction in the Molten Salt Fast Reactor: analytical, deterministic and Monte Carlo approaches. Ann. Nucl. Energy 65, 78–90.

Aufiero, M., Cammi, A., Geoffroy, O., Losa, M., Luzzi, L., Ricotti, M., Rouch, H., 2014b. Development of an OpenFOAM model for the Molten Salt Fast Reactor transient analysis. Chem. Eng. Sci. 111, 390–401.

Bell, G., Glasstone, S., 1970. Nuclear Reactor Theory. Van Nostrand Reinhold Co., New York.

Bowman, R.A., Müller, A.C., Nagle, W., 1940. Mean temperature difference in design. Trans. ASME 62, 283–293.

Briggs, R.B., 1964. Molten-Salt Reactor Program. Technical report, ORNL-3708.

Cammi, A., Di Marcello, V., Luzzi, L., Memoli, V., 2011a. The multi-physics modelling approach oriented to safety analysis of innovative nuclear reactors. In: Acosta, M.J. (Ed.), Advances in Energy Research, vol. 5. Nova Science Publishers Inc., Hauppauge, NY, pp. 171–214.

Cammi, A., Di Marcello, V., Luzzi, L., Memoli, V., Ricotti, M.E., 2011b. A multi-physics modelling approach to the dynamics of molten salt reactors. Ann. Nucl. Energy 38, 1356–1372.

Cammi, A., Fiorina, C., Guerrieri, C., Luzzi, L., 2012. Dimensional effects in the modelling of MSR dynamics: moving on from simplified schemes of analysis to a multi-physics modelling approach. Nucl. Eng. Des. 246, 12–26.

Comsol, 2012a. CFD Module User's Guide. COMSOL, Inc. version 4.3a.

Comsol, 2012b. COMSOL Multiphysics User's Guide. COMSOL, Inc. version 4.3a.

Dulla, S., Ravetto, P., 2007. Interactions between fluid-dynamics and neutronics phenomena in the physics of molten-salt systems. Nucl. Sci. Eng. 155, 475–488.

Dulla, S., Ravetto, P., Rostagno, M.M., 2004. Neutron kinetics of fluid-fuel systems by the quasi-static method. Ann. Nucl. Energy 31, 1709–1733.
Fiorina, C., Aufiero, M., Cammi, A., Franceschini, F., Krepel, J., Luzzi, L., Mikityuk, K., Ricotti, M.E., 2013. Investigation of the MSFR core physics and fuel cycle char-acteristics. Prog. Nucl. Energy 68 (0), 153–168.
Fiorina, C., Cammi, A., Guerrieri, C., Luzzi, L., Spinelli, B., 2010. Development of a simulation tool for a preliminary analysis of the MSR core dynamics. In: Proceedings of the International Conference Nuclear Energy for New Europe 2010 (NENE 2010), Portorož, Slovenia, September 6–9, 2010, pp. 105.1–105.9.
Fiorina, C., Lathouwers, D., Aufiero, M., Cammi, A., Guerrieri, C., Kloosterman, J., Luzzi, L., Ricotti, M., 2014. Modelling and analysis of the MSFR transient behaviour. Ann. Nucl. Energy 64, 485–498.
Furukawa, K., Arakawa, K., Erbay, L.B., Ito, Y., Kato, Y., Kiyavitskaya, H., Lecocq, A., Mitachi, K., Moir, R., Numata, H., Pleasant, J.P., Sato, Y., Shimazu, Y., Simonenco, V.A., Sood, D.D., Urban, C., Yoshioka, R., 2008. A road map for the realization of global-scale thorium breeding fuel cycle by single molten-fluoride flow. Energy Convers. Manag. 49, 1832–1848.
Fütterer, M., 2008. Adaptive control of simulated moving bed plants using COMSOL's Simulink interface. In: Proceedings of the European COMSOL Conference, Hannover, Germany, November 23–24, 2008.
Gabbard, C.H., 1970. Reactor Power Measurement and Heat Transfer Performance in the Molten Salt Reactor Experiment. Technical report. ORNL-TM-3002.
GIF, 2002. A Technology Roadmap for Generation IV Nuclear Energy Systems. GIF-002-00. US DOE Nuclear Energy Research Advisory Committee and the Generation IV International Forum.
GIF, 2014. Technology Roadmap Update for Generation IV Nuclear Energy Systems. Available at: https://www.gen-4.org/gif/upload/docs/application/pdf/2014-03/gif-tru2014.pdf.
Grimes, W.R., 1970. Molten-salt reactor chemistry. Nucl. Technol. 8, 137–155. Guo, Z., Zhou, J., Zhang, D., Chaudri, K., Tian, W., Su, G., Qiu, S., 2013. Coupled neutronics/thermal-hydraulics for analysis of molten salt reactor. Nucl. Eng. Des. 258, 144–156.
Guerrieri, C., Cammi, A., Fiorina, C., Luzzi, L., 2010. A multi-physics numerical model for the MSR core dynamics. In: Proceedings of International Conference Nuclear Energy for New Europe 2010 (NENE 2010), Portorož, Slovenia, September 6–9, 2010, pp. 102.1–102.11.
Guerrieri, C., Fiorina, C., Cammi, A., Luzzi, L., 2011. Preliminary assessment of modelling issues related to the dynamics and control of graphite-moderated MSR. In: Proceedings of the International Congress on Advances in Nuclear Power Plants (ICAPP 2011), Nice, France, May 2–5, 2011. Paper 11099.
Guymon, R.H., 1973. MSRE Systems and Components Performance. Technical report, ORNL-TM-3039.
Haubenreich, P.N., Engel, J.R., 1970. Experience with the molten salt reactor experiment. Nucl. Technol. 8, 118–136.
Henry, A.F., 1958. The application of reactor kinetics to the analysis of experiments. Nucl. Sci. Eng. 3, 52–70.
Hetrick, D., 1972. Dynamics of Nuclear Systems. University of Arizona Press, La Grange Park, IL.
Hron, M., 2005. Project SPHINX spent hot fuel incinerator by neutron flux (the development of a new reactor concept with liquid fuel based on molten fluorides). Prog. Nucl. Energy 47, 347–353.
Kedl, R.J., 1970. Fluid Dynamic Studies of the Molten-Salt Reactor Experiment (MSRE) Core. Technical report, ORNL-TM-3229.
Kópházi, J., Lathouwers, D., Kloosterman, J.L., 2009. Development of a three-dimensional time-dependent calculation scheme for molten salt reactors and validation of the measurement data of the molten salt reactor experiment. Nucl. Sci. Eng. 163, 118–131.
Krepel, J., Grundmann, J., Rohde, U., Weiss, F.P., 2005. DYN1D-MSR dynamics code for molten salt reactors. Ann. Nucl. Energy 32, 1799–1824.
Krepel, J., Hombourger, B., Fiorina, C., Mikityuk, K., Rohde, U., Kliem, S., Pautz, A., 2014a. Fuel cycle advantages and dynamics features of liquid fueled MSR. Ann. Nucl. Energy 64, 380–397.
Krepel, J., Mikityuk, K., Hombourger, B., Pautz, A., Zanetti, M., Aufiero, M., Luzzi, L., 2014b. Hybrid spectrum molten salt reactor. In: Proceedings of the International Conference PHYSOR 2014, Kyoto, Japan, September 28–October 3, 2014.
Krepel, J., Rohde, U., Grundmann, U., Weiss, F.P., 2007. DYN3D-MSR spatial dynamics code for molten salt reactors. Ann. Nucl. Energy 34, 449–462.
Lapenta, G., Mattioda, F., Ravetto, P., 2001. Point kinetic model for fluid fuel systems. Ann. Nucl. Energy 28, 1759–1772.
Lapenta, G., Ravetto, P., 2000. Basic reactor physics problems in fluid-fuel recirculated reactors. Kerntechnik 65, 250–253.
LeBlanc, D., 2010. Molten salt reactors: a new beginning for an old idea. Nucl. Eng. Des. 240, 1644–1656.
Lecarpentier, D., Carpentier, V., 2003. A neutronics program for critical and nonequilibrium study of mobile fuel reactors: the Cinsf1D code. Nucl. Sci. Eng. 143, 33–46.
Leppänen, J., 2007. Development of a New Monte Carlo Reactor Physics Code (Ph.D. thesis). Helsinki University of Technology.
Li, L., Yang, J.D., 2010. Advanced simulation of hydroelectric transient process with COMSOL/Simulink. In: IOP Conference Series: Earth and Environmental Science, vol. 12, 012060.
Luzzi, L., Aufiero, M., Cammi, A., Fiorina, C., 2012a. Thermo-hydrodynamics of internally heated molten salts for innovative nuclear reactors. In: Zheng, Jinhai (Ed.), Hydrodynamics – Theory and Model. InTech, Rijeka, Croatia, pp. 119–142 (Chapter 6).
Luzzi, L., Di Marcello, V., Cammi, A., 2012b. Multi-Physics Approach to the Modeling and Analysis of Molten Salt Reactors. In: Physics Research and Technology Se-ries. Nova Science Publishers, Inc., New York, NY, pp. 1–140.
MacPherson, H.G., 1985. The molten salt reactor adventure. Nucl. Sci. Eng. 90, 374–380.
Mengali, M., Lanfredini, M., Moretti, F., D'Auria, F., 2012. Technical Report, ENEA XCIRTEN-LP3-014. Available in English at: http://hdl.handle.net/10840/4449. Mathieu, L., Heuer, D., Brissot, R., Le Brun, C., Liatard, E., Loiseaux, J.M., Méplan, O., Merle-Lucotte, E., Nuttin, A., Wilson, J., Garzenne, C., Lecarpentier, D., Walle, E., 2006. The thorium molten salt reactor: moving on from the MSBR. Prog. Nucl. Energy 48, 664–679.
Mathieu, L., Heuer, D., Merle-Lucotte, E., Brissot, R., Le Brun, C., Liatard, E., Loiseaux, J.-M., Méplan, O., Nutti, A., Lecarpentier, D., 2009. Possible configurations for the thorium molten salt reactor and advantages of the fast non-moderated version. Nucl. Sci. Eng. 161, 78–89.
Matlab, 2012. Simulink User's Guide. The Mathworks, Inc. r2012b Edition. Mattioda, F., Ravetto, P., Ritter, G., 2000. Effective delayed neutron fraction for fluid-fuel systems. Ann. Nucl. Energy 27, 1523–1532.
Merle-Lucotte, E., Heuer, D., Allibert, M., Brovchenko, M., Capellan, N., Ghetta, V., 2011. Launching the thorium fuel cycle with the Molten Salt Fast Reactor. In: Proceedings of International Congress on Advances in Nuclear Power Plants (ICAPP 2011), Nice, France, May 2–5, 2011. Paper 11190.
Merle-Lucotte, E., Heuer, D., Allibert, M., Ghetta, V., Le Brun, C., 2008. Introduction to the physics of molten salt reactor. Materials Issues for Generation IV Systems. In: NATO Science for Peace and Security Series – B. Editions Springer, pp. 501–521.
Mylonakis, A.G., Varvayanni, M., Catsaros, N., Savva, P., Grigoriadis, D.G.E., 2014. Multi-physics and multi-scale methods used in nuclear reactor analysis. Ann. Nucl. Energy 72, 104–119.
Nagy, K., Lathouwers, D., T'Joen, C., Kloosterman, J., van der Hagen, T., 2014. Steady-state and dynamic behavior of a moderated molten salt reactor. Ann. Nucl. Energy 64, 365–379.
Nicolino, C., Lapenta, G., Dulla, S., Ravetto, P., 2008. Coupled dynamics in the physics of molten salt reactors. Ann. Nucl. Energy 35, 314–322.
Quarteroni, A., Veneziani, A., 2003. Analysis of a geometrical multiscale model based on the coupling of ODE and PDE for blood flow simulations. Multiscale Model. Simul. 1 (2), 173–195.
Renault, C., Delpech, S., Merle-Lucotte, E., Konings, R., Hron, M., Ignatiev, V., 2009. The molten salt reactor: R&D status and perspectives in Europe. In: Proceedings of the 7th European Commission Conference on Euratom Research and Training in Reactor Systems (FISA 2009), Prague, Czech Republic, pp. 384–399.
Robertson, R.C., 1965. MSRE Design and Operations Report Part I: Description of Reactor Design. Technical report, ORNL-TM-0728.
Samulon, H.A., 1951. Spectrum analysis of transient response curves. Proc. Inst. Radio Eng. (IRE) 39 (2), 175–186.
Schijndel, A., 2009. Integrated modeling of dynamic heat, air and moisture processes in buildings and systems using Simulink and COMSOL. Build. Simul. 2, 143–155.
Serp, J., Allibert, M., Benes, O., Delpech, S., Feynberg, O., Ghetta, V., Heuer, D., Holcomb, D., Ignatiev, V., Kloosterman, J.L., Luzzi, L., Merle-Lucotte, E., Uhlir, J., Yoshioka, R., Zhimin, D., 2014. The molten salt reactor (MSR) in generation IV: overview and perspectives. Prog. Nucl. Energy 77, 308–319.
Steffy, R.C., 1970a. Experimental Dynamic Analysis of the MSRE with 233U Fuel. Technical report, ORNL-TM-2997.
Steffy, R.C., 1970b. Frequency Response Testing of the Molten-Salt Reactor Experiment. Technical report, ORNL-TM-2823.
Suzuki, N., Shimazu, Y., 2006. Preliminary safety analysis on depressurization accident without scram of a molten salt reactor. Nucl. Sci. Eng. 43, 720–730.
Suzuki, N., Shimazu, Y., 2008. Reactivity-initiated-accident analysis without scram of a molten salt reactor. Nucl. Sci. Eng. 45, 575–581.
Thoma, R.E., 1971. Chemical Aspects of MSRE Operations. Technical report, ORNL-4658.
Uhlíř, J., 2007. Chemistry and technology of molten salt reactors – history and perspectives. J. Nucl. Mater. 360, 6–11.
Wang, S., Rineiski, A., Maschek, W., 2006. Molten salt related extensions of the SIMMER-III code and its application for a burner reactor. Nucl. Eng. Des. 236, 1580–1588.
Yamamoto, T., Mitachi, K., Ikeuchi, K., Suzuki, T., 2006. Transient characteristics of small molten salt reactor during blockage accident. Heat Transf. Asian Res. 35, 434–450.
Yamamoto, T., Mitachi, K., Suzuki, T., 2005. Steady state analysis of small molten salt reactor. JSME Int. J. Ser. B 48, 610–717.
Zanetti, M., Luzzi, L., Cammi, A., Fiorina, C., 2014. An innovative approach to dynamics modeling and simulations of the molten salt reactor experiment. In: Proceedings of the International Conference PHYSOR 2014, Kyoto, Japan, September 28–October 3, 2014.
Zhang, D., Guo, Z., Wang, C., Qiu, S., Zhai, Z.G., Rineiski, A., Wang, S., 2014. Fluent-based neutronics and thermal-hydraulics coupling calculation for a liquid-fuel molten salt reactor. In: Proceedings of the 10th International Topical Meeting

on Nuclear Thermal-Hydraulics, Operation and Safety (NUTHOS-10), Okinawa, Japan, December 14–18, 2014. Paper 1145.
Zhang, D.L., Qiu, S.Z., Su, G.H., 2009a. Development of a safety analysis code for molten salt reactors. Nucl. Eng. Des. 239, 2778–2785.
Zhang, D.L., Qiu, S.Z., Su, G.H., Liu, C.L., 2009b. Development of a steady state analysis code for a molten salt reactor. Ann. Nucl. Energy 36, 590–603.
Zhang, D.L., Qiu, S.Z., Su, G.H., Liu, C.L., Qian, L.B., 2009c. Analysis on the neutron kinetics for a molten salt reactor. Prog. Nucl. Energy 51, 624–636.